Liquid Crystals
Publication details, including instructions for authors and subscription information:
http://www.informaworld.com/smpp/title~content=t713926090

Phase behaviour of the thermotropic cubic mesogens 1,2-bis-(4-*n*-undecyl- and 4-*n*-dodecyl-oxybenzoyl)hydrazine under pressure

Yoji Maeda Corresponding author[a]; Takeya Ito[b]; Shoichi Kutsumizu[b]
[a] Nanotechnology Research Institute, National Institute of Advanced Industrial Science and Technology, Ibaraki 305-8565, Japan [b] Department of Chemistry, Faculty of Engineering, Gifu University, Gifu 501-1193, Japan

Online publication date: 25 May 2010

To cite this Article Maeda Corresponding author, Yoji , Ito, Takeya and Kutsumizu, Shoichi(2004) 'Phase behaviour of the thermotropic cubic mesogens 1,2-bis-(4-*n*-undecyl- and 4-*n*-dodecyl-oxybenzoyl)hydrazine under pressure', Liquid Crystals, 31: 6, 807 — 820
To link to this Article: DOI: 10.1080/02678290410001697549
URL: http://dx.doi.org/10.1080/02678290410001697549

LIQUID CRYSTALS, 2004, VOL. 31, NO. 6, 807–820

Phase behaviour of the thermotropic cubic mesogens 1,2-bis-(4-*n*-undecyl- and 4-*n*-dodecyl-oxybenzoyl)hydrazine under pressure

YOJI MAEDA*

Nanotechnology Research Institute, National Institute of Advanced Industrial Science and Technology, Higashi 1-1, Tsukuba, Ibaraki 305-8565, Japan

TAKEYA ITO and SHOICHI KUTSUMIZU

Department of Chemistry, Faculty of Engineering, Gifu University, 1-1 Yanagido, Gifu 501-1193, Japan

(*Received 5 January 2004; accepted 12 February 2004*)

The phase transition behaviour of two optically isotropic, thermotropic cubic mesogens 1,2-bis-(4-*n*-undecyloxy- and 4-*n*-dodecyloxy-benzoyl)hydrazine, BABH(11) and BABH(12), was investigated under hydrostatic pressures up to 300 MPa using a high pressure differential thermal analyser, a wide angle X-ray diffractometer and a polarizing optical microscope equipped with a high pressure optical cell. It is found that for BABH(11) and BABH(12), a smectic C (SmC) phase is induced between the isotropic liquid (I) and the cubic (Cub) phases by applying pressures above 10–12 and 16–17 MPa, respectively. A sea–island texture consisting of bright sand-like sea regions (SmC phase) and areas of dark islands (Cub phase) appears in the mesophase under pressures up to 140 MPa, while the sand-like texture of the SmC phase is formed predominantly on cooling under pressure. These observations indicate the destabilization of the cubic phase with increasing pressure. The phase transition sequence of BABH(11) and BABH(12), Cr–Cub–I at atmospheric pressure, changes to Cr–Cub–SmC–I under intermediate pressures and would change to Cr–SmC–I under elevated pressure.

1. Introduction

In 1978, 1,2-bis-(4-*n*-alkyloxybenzoyl)hydrazines, referred to as BABH(*n*) where *n* indicates the number of carbon atoms in the alkoxy chain, were synthesized by Schubert *et al*. [1] and for the octyloxy-, nonyloxy- and decyloxy-homologues optically isotropic phases were found. As shown by Demus *et al*. [2], these homologues exhibit both cubic (Cub) and smectic C (SmC) phases, and show the phase sequence crystal (Cr_I)–crystal (Cr_{II})–Cub–SmC–isotropic liquid (I). The chemical structure of the 1,2-bis-(4-*n*-alkoxybenzoyl)-hydrazines BABH(*n*) is:

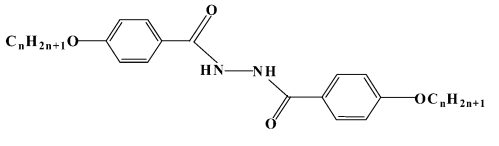

The jointed rod model [3, 4], i.e. rods linked three-by-three forming two networks interwoven but not connected, is the generally accepted explanation of the cubic structure with the space group *Ia*3*d* in lyotropic systems [3–10]. It is widely accepted that the interface between the hydrophilic part of the amphiphilic molecules and the water molecules builds an infinite bicontinuous periodic minimal surface (IPMS), which divides space into two parts [8–10]. The three simplest cubic IPMS have been shown mathematically to be the Schöen Gyroid G (space group *Ia*3*d*), and the P and D Schwarz surfaces (space groups *Im*3*m* and *Pn*3*m*), respectively [11–14]. The space group *Ia*3*d* is related to the gyroid G in which the IPMS forms two interwoven labyrinths, each of which consists of rods linked three-by-three. The diffracted intensity by a G surface decorated by a layer was calculated and the theoretical predictions fit with the experimental data obtained for direct and inverted *Ia*3*d* cubic mesophases [15]. The application of this model to thermotropic cubic phases requires the formation of rods by molecules of the pure compounds.

The structure of the crystal as well as of the cubic and SmC phases of BABH(8) has been determined [2, 16], and the cubic phase has a body-centered cubic cell ($a = 6.46$ nm) with the space group *Ia*3*d* or *I*43*d* [16]. Recently a quasi-binary (QB) picture [17, 18] for the

*Author for correspondence; e-mail: yoji.maeda@aist.go.jp

Liquid Crystals ISSN 0267-8292 print/ISSN 1366-5855 online © 2004 Taylor & Francis Ltd
http://www.tandf.co.uk/journals
DOI: 10.1080/02678290410001697549

thermotropic cubic systems has been proposed on the basis of thermodynamic observations [19–24]. The experimental conformational entropy of the long alkyl chains attached to the rigid core of these mesogenic molecules indicates that the alkyl chains are highly disordered in the liquid crystalline states. The disordered alkyl chains are treated as an 'intramolecular solvent' or 'self-solvent' based on the strong similarity between the phase diagrams of neat and binary systems. The QB picture is shown to be applicable to the classic examples of thermotropic cubic phases: the essential structural motif is TPMS (or IPMS) surface.

The authors have reported the phase behaviour of BABH(8) and BABH(10) under pressure using a high pressure differential thermal analyser (DTA) and a polarizing optical microscope (POM) equipped with a high pressure optical cell, and determined the T vs. P phase diagram in the heating mode [25, 26]. Since only the Cub–SmC transition line of all the phase boundaries has a negative slope (dT/dP) in the T–P phase diagram, the temperature range for the cubic phase decreases rapidly with pressure. A triple point for the SmC, Cub and Cr phases is estimated as 31.6 MPa, 147°C in BABH(8) and 10–11 MPa, 144 ± 1°C in BABH(10), indicating the upper limit of pressure for the observation of the cubic phase. The phase transition sequence, low temperature crystal (Cr_2)–high temperature crystal (Cr_1)–Cub–SmC–I observed in the low pressure region changes to Cr_2–SmC–I in the high pressure region. The structures and optical texture of the cubic and SmC phases change reversibly from the spot-like X-ray pattern and the dark field of view for the cubic phase to the Debye–Sherrer pattern and the sand-like texture for the SmC phase, both in isobaric and isothermal experiments. BABH(n) compounds with longer alkyl chains ($n > 10$) have also been synthesized and BABH(11), BABH(12) and BABH(14) are found to show only the cubic phase between the crystalline solid and isotropic liquid [27]. The interesting phase behaviour of BABH(8) and BABH(10) under pressure prompted us to study the phase behaviour of BABH(n) compounds with longer alkoxy chains ($n > 10$) under hydrostatic pressure, focusing in particular on the effect of pressure on the stability of the cubic phase.

In this paper, we present the experimental results on the thermal, morphological and structural behaviour of BABH(11) and BABH(12) under hydrostatic pressures up to 300 MPa using a high pressure DTA, a POM equipped with a high pressure optical cell, and a wide angle X-ray diffractometer (WAXD) equipped with a high pressure vessel.

2. Experimental

2.1. *Sample characterization under ambient pressure*

BABH(11) and BABH(12), prepared as described in [1, 27], were used in this study. Samples had been recrystallized from ethanol several times and the purity was confirmed by infrared (IR), ^{1}H NMR and mass spectroscopies, and by elemental analysis. Thermal characterization was performed on a Perkin-Elmer DSC-7 and Seiko Instruments SSC-5000 differential scanning calorimeters at a scanning rate of 5°C min^{-1} under N_2 gas flow. Temperatures and heats of transition were calibrated using standard materials (indium and tin). Transition temperatures were determined as the onset of the transition peaks at which the tangential line of the inflection point of the rising part of the peak crosses the extrapolated baseline. Morphological characterization was performed using a Leiz Orthoplan POM equipped with a Mettler hot stage FP-82.

2.2. *DTA measurements under pressure*

The high pressure DTA apparatus used in this study has been described elsewhere [28]. The DTA system was operated in a temperature region between room temperature and 250°C under hydrostatic pressures up to 300 MPa. Dimethylsilicone oil with a medium viscosity (100 cSt) was used as the pressurizing medium. The sample was placed in the sample cell and coated with an epoxy adhesive, to fix the sample in the bottom of the cell and also to prevent direct contact with the silicone oil. A new specimen was used for each DTA measurement. The DTA runs were performed at a constant heating rate of 5°C min^{-1} under various pressures. Peak temperatures were used as transition temperatures in constructing the real temperature vs. pressure phase diagram. When estimating specific points such as a triple point, the transition temperature was corrected to become the onset temperature by subtracting a temperature difference between the onset and peak temperatures, of about 3.5°C.

2.3. *Morphological and X-ray characterization under pressure*

The observation of optical texture under hydrostatic pressure was performed using a Leitz Orthoplan POM equipped with a high pressure optical cell system [29]. Transmitted light intensity through the POM with crossed Nicols was measured using a Mettler FP-90 photomonitor under atmospheric and hydrostatic pressures. The texture observation was performed at isobaric and isothermal conditions in the pressure range up to 50 MPa.

Structural changes during the phase transitions of BABH(12) under pressure were observed using a high

pressure WAXD apparatus [28]. The high pressure vessel was set on the wide angle goniometer of a 12 kW rotating anode X-ray generator (Rotaflex RU200, Rigaku Co.). The sample was inserted into the vertical hole of the beryllium spindle as the sample cell. The beryllium spindle was mechanically compressed for pressure sealing using upper and lower pressure blocks. The sample was then pressurized hydrostatically at pressures up to 200 MPa. A Ni-filtered Cu K_α X-ray beam was used to irradiate the sample, and diffraction patterns were obtained using an imaging plate detector (BAS-IP $127 \times 127\,mm^2$, Fuji Photo Film Co.).

3. Results and discussion

3.1. *Characterization of BABH(11) and BABH(12) at atmospheric pressure*

Figure 1 shows the DSC heating curves of BABH(11) and BABH(12) at a heating rate of $5^\circ C\,min^{-1}$, showing the Cr–Cub–I transition sequence: Cr_3–54.1°C–Cr_2–126.1°C–Cr_1–138.3°C–Cub–163.0°C–I for BABH(11) and Cr_3–100°C–Cr_2–128.9°C–Cr_1–135.5°C–Cub–161.7°C–I for BABH(12). The table lists the thermodynamic quantities associated with the phase transitions of BABH(11) and BABH(12). Figure 2 shows the X-ray pattern of the cubic phase of BABH(12) at 150°C in the cooling mode at atmospheric pressure. The spot-like reflections indicate a polydomain structure, as already seen for the cubic phases of BABH(8) and BABH(10) [25, 26]. The pattern of diffraction spots of the cubic phase is very similar to that for BABH(8) which reduced to the {2 1 1} and {2 2 0} reflections of the cubic phase with space group *Ia*3*d* [16].

3.2. *Thermal behaviour of BABH(11) and BABH(12) under pressure*

The thermal behaviour of BABH(11) and BABH(12) was investigated under pressure to study the effect of

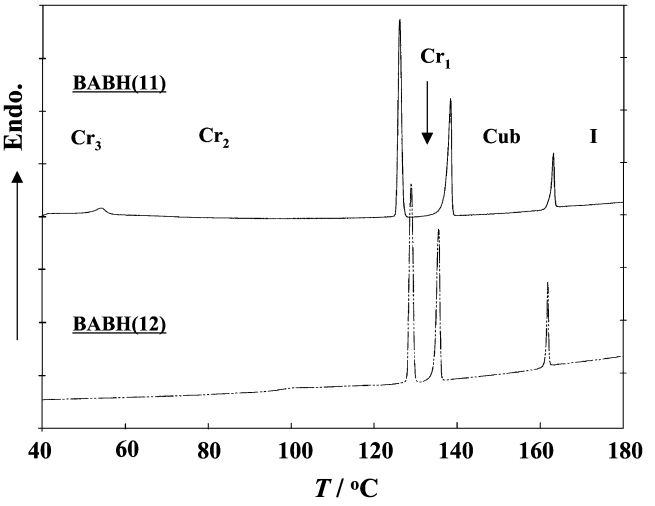

Figure 1. DSC heating and cooling curves for BABH(11) and BABH(12). Scanning rate: $5^\circ C\,min^{-1}$.

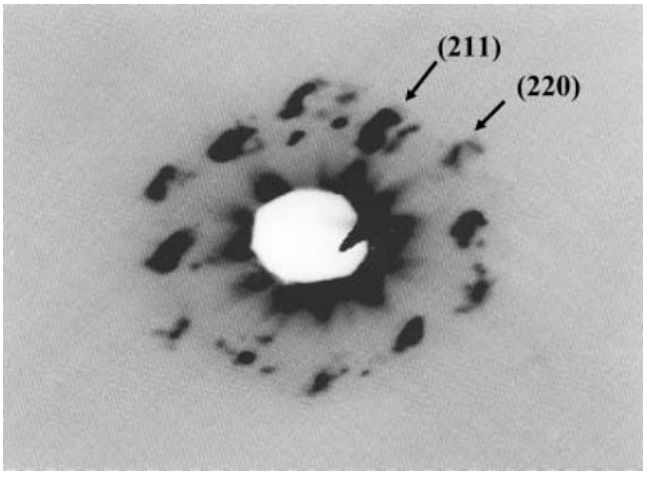

Figure 2. X-ray diffraction pattern of the cubic phase shown by BABH(12) at 150°C on cooling from the isotropic liquid.

Table 1. Thermodynamic quantities associated with the phase transitions of BABH(11) and BABH(12).

Phase transition	T^*/°C[a]	ΔH/kJ mol^{-1}	ΔS/J K^{-1} mol^{-1}	$(dT/dP)_{1atm}$	ΔV/cm^{3}mol^{-1}
BABH(11)					
$Cr_3 \rightarrow Cr_2$	51.4	3.3	10.2	—	—
$Cr_2 \rightarrow Cr_1$	125.3	30.9	77.6	0.295_1	22.9
$Cr_1 \rightarrow$Cub	137.1	22.6	55.1	0.273_2	15.1
Cub→I	162.3	7.4	17.0	0.263_4	4.5
BABH(12)					
$Cr_3 \rightarrow Cr_2$	*c* 100	—	—	—	—
$Cr_2 \rightarrow Cr_1$	128.1	33.9	84.5	0.401_9	34.0
$Cr_1 \rightarrow$Cub	134.6	24.8	60.9	0.246_1	15.0
Cub→I	161.2	7.1	16.4	0.268_6	4.4

[a] T^* is the temperature of the onset of the transition peak, i.e. the temperature at which the tangential line of the inflection point of the rising part of the peak intersects the extrapolated baseline.

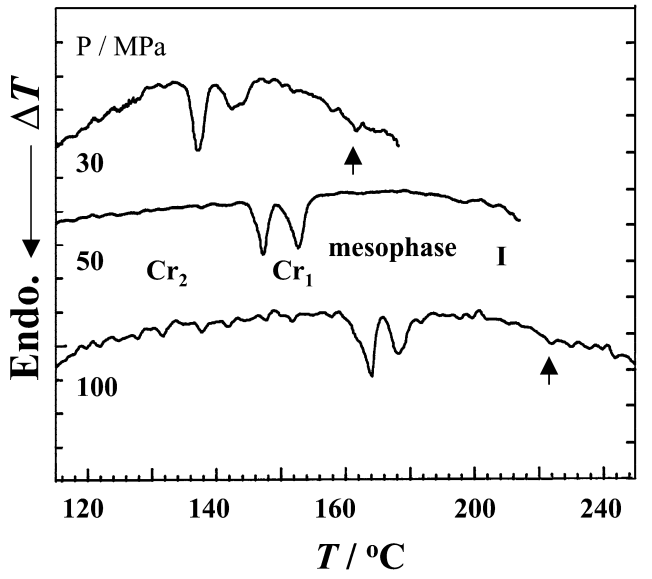

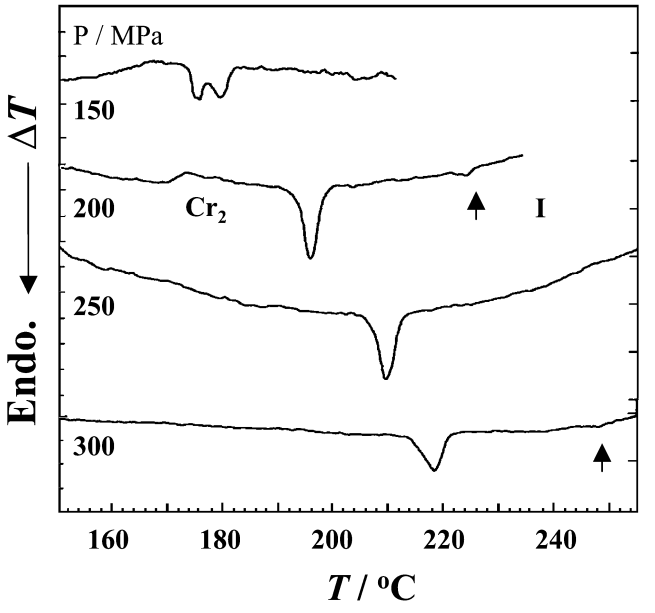

Figure 3. DTA heating curves of BABH(11) at various pressures. Heating rate: 5°C min^{-1}.

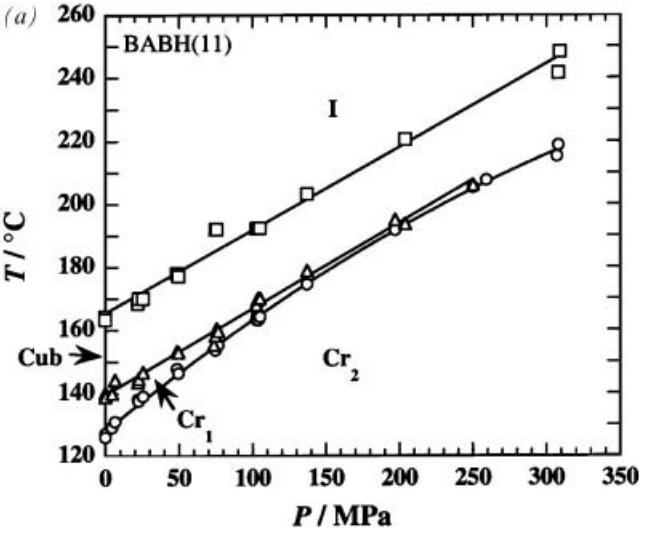

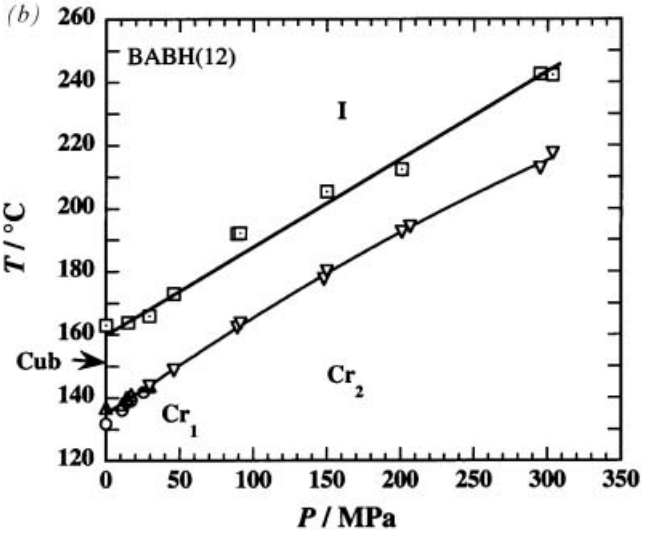

Figure 4. *T*–*P* phase diagrams of (*a*) BABH(11) and (*b*) BABH(12) constructed in the heating mode using the high-pressure DTA.

pressure on the phase stability of the cubic phase. Figure 3 shows the DTA heating curves of BABH(11) at various pressures. The heating curves show a strong double peak associated with the main transitions and a smaller peak at higher temperatures; these are assigned as the $Cr_2 \rightarrow Cr_1$ and $Cr_1 \rightarrow$mesophase transitions for the double peak and the mesophase$\rightarrow$I transition, respectively. The double peak begins to close and then merges to an apparently single peak at higher pressures of above 200 MPa. Initially, the mesophase seemed to be the cubic phase over the whole pressure region because there is no mesophase transition under hydrostatic pressures. The thermal behaviour of BABH(12) under pressures is very similar to that of BABH(11). Figure 4 shows the T vs. P phase diagrams of BABH(11) and BABH(12) in the pressure range up to 300 MPa. The transition curves can be expressed approximately by either first or second order polynomials in terms of pressure as follows:

BABH(11) (T/°C = peak temperature)

$Cr_2 \rightarrow Cr_1$ $T/°C = 128.1 + 0.380_8\ (P/\text{MPa}) - 2.956_9 \times 10^{-4}\ (P/\text{MPa})^2$

$Cr_1 \rightarrow$Cub(SmC) $T/°C = 139.5 + 0.273_2\ (P/\text{MPa})$

$Cub(SmC) \rightarrow I \quad T/^{\circ}C = 165.5 + 0.263_4 \ (P/MPa)$

BABH(12)

$Cr_2 \rightarrow Cr_1 \quad T/^{\circ}C = 131.9 + 0.401_9 \ (P/MPa)$

$Cub(SmC) \rightarrow I \quad T/^{\circ}C = 162.4 + 0.268_6 \ (P/MPa)$

$0 < P < 30\,MPa$

$Cr_1 \rightarrow Cub \quad T/^{\circ}C = 136.4 + 0.246_1 \ (P/MPa)$

$30 < P < 300\,MPa$

$Cr_1 \rightarrow SmC \quad T/^{\circ}C = 134.3 + 0.331_9 \ (P/MPa) - 2.063_4 \times 10^{-4} \ (P/MPa)^2$

No mesophase transition for either BABH(11) or BABH(12) was detected by the DTA measurements at any pressure, but a new phase is pressure-induced on applying pressure, as will be described in the next paragraph. The morphological and structural evidence for the SmC phase was obtained using *in situ* POM observations and X-ray diffraction measurements under hydrostatic pressure. Thus the $Cr_1 \rightarrow Cub(SmC)$ transition line described previously means that the $Cr_1 \rightarrow Cub$ transition line in the low pressure region connects smoothly to the $Cr_1 \rightarrow SmC$ transition line in the high pressure region. The boundary exists at about 10–12 MPa for BABH(11) and 16–17 MPa for BABH(12), as will be explained in the next paragraph. On the other hand, an intersection between the Cr_2–Cr_1 and Cr_1–Cub transition lines is expected at about 90.4 and 28.5 MPa for BABH(11) and BABH(12), respectively, indicating the upper limit of pressure for the observation of the Cr_1 phase.

3.3. *Morphological and structural observations under pressure*

The POM observations of BABH(11) and BABH(12) at atmospheric pressure show simply the change in texture between the black field of view for the cubic phase (and also the isotropic liquid) and the crystalline spherulites. The *in situ* observations of the textures of BABH(11) and BABH(12) under pressure were performed both on isobaric and isothermal paths, to characterize the texture of the mesophase under pressure. The same transitions as those seen at atmospheric pressure are observed under very low pressures below 10 and 15 MPa for BABH(11) and BABH(12), respectively, although the black fields of view for the cubic phase and isotropic liquid are not black, but dark brown under hydrostatic pressure. Figure 5 shows the textures of BABH(12) in the heating mode at 15 MPa. The spherulitic texture, figure 5 (*a*), of the crystal (Cr) at 30°C persists to temperatures of 137–138°C, at which temperature the crystalline texture changes to a ripple- or mesh-like one for the cubic phase, figures 5 (*c*) and 5 (*d*). The ripple- or mesh-like texture of the cubic phase is maintained to just before the isotropization temperature. Such a ripple- or mesh-like texture is commonly observed for the cubic phases of BABH(11) and BABH(12) on heating under pressure. The mesh-like texture of the cubic phase reflects the polydomain structure resulting from the crystalline spherulites, and such a texture is often not seen on cooling from the isotropic liquid. The mesh-like pattern is broken at 159°C, figure 5 (*e*), due to isotropization and disappears completely to the dark featureless texture of the isotropic liquid at 160°C, figure 5 (*f*). Slightly increasing the pressure induces an entirely different texture in the mesophase.

Figure 6 shows the textures of BABH(12) in the heating mode at 30 MPa. The spheruitic texture, figure 6 (*a*), of the crystal persists to temperatures of 138–139°C. An unusual pattern, figure 6 (*b*), is observed at 140°C in which several parts of the spherulite become black during the Cr–Cub transition. A sea–island texture is observed at 143°C, figure 6 (*c*), and remains to about 160°C. The bright sea and dark islands are the SmC and Cub phases, respectively. Then the dark field of view expands from the dark islands by consuming parts of the bright sea (SmC phase) at 165°C, figure 6 (*e*); finally the bright sand-like texture changes completely into the dark featureless field of view of the isotropic liquid at 167°C, figure 6 (*f*).

When the sample is cooled from the isotropic liquid at 168°C, figure 7 (*a*), bright sand-like spheres, figure 7 (*b*), are formed in the dark field of view of the isotropic liquid at 166°C. This clearly reveals the pressure-induced formation of the SmC phase and is the same texture as observed in BABH(8) and BABH(10) [25, 26]. The bright islands grow rapidly with decreasing temperature, figures 7 (*c*) and 7 (*d*), and coalesce to form the homogeneous sand-like texture of the SmC phase at 157°C, figure 7 (*e*), although small black spots randomly placed of the cubic phase remain. Crystals, figure 7 (*f*), are formed on cooling, immediately after the appearance of the dark brown field of view of the cubic phase.

The morphological changes on heating and cooling at 30 MPa indicate the reversiblity of the transition sequence, I–SmC–Cub–Cr for BABH(12), which is the same as that of BABH(8) and BABH(10) observed under atmospheric pressure. Also in BABH(11) the pressure-induced SmC phase appears on cooling from the isotropic liquid at pressures above about 10 MPa. It is interesting that the bright sea–dark island texture of BABH(12), indicating SmC and cubic phases, respectively, is very similar to that observed in BABH(10), but is inverted in composition: specifically for BABH(10), the bright islands are the SmC phase while the dark sea is the cubic phase. Since the sea component is the major phase under each set of

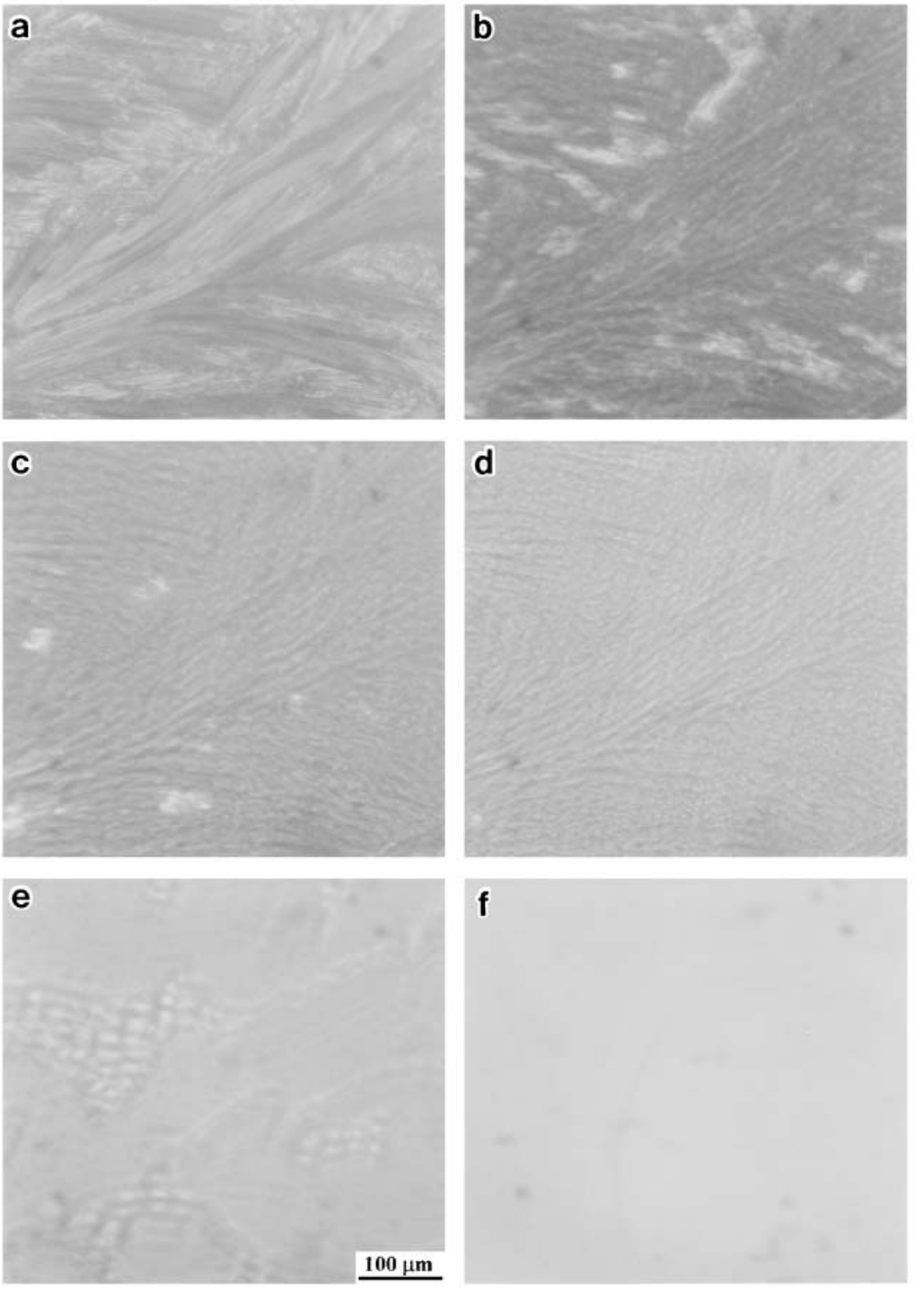

Figure 5. POM photographs of BABH(12) on heating at 15 MPa: (*a*) Cr_3 at 30°C; (*b*) Cr_1 at 138°C; (*c*) Cub phase at 139°C; (*d*) Cub phase at 140°C; (*e*) Cub–I transition at 159°C; (*f*) isotropic liquid at 160°C.

conditions, the pressure-induced SmC phase of BABH(12) has greater stability at 30 MPa.

Figure 8 shows the pressure dependence of the textures of the cubic phase of BABH(11) at 140°C on an isothermal path. The mesh-like texture of the cubic phase persists for pressures up to 11 MPa, figures 8 (*a*) and 8 (*b*). These meshes show irregular shapes with the short and long axes of several microns and

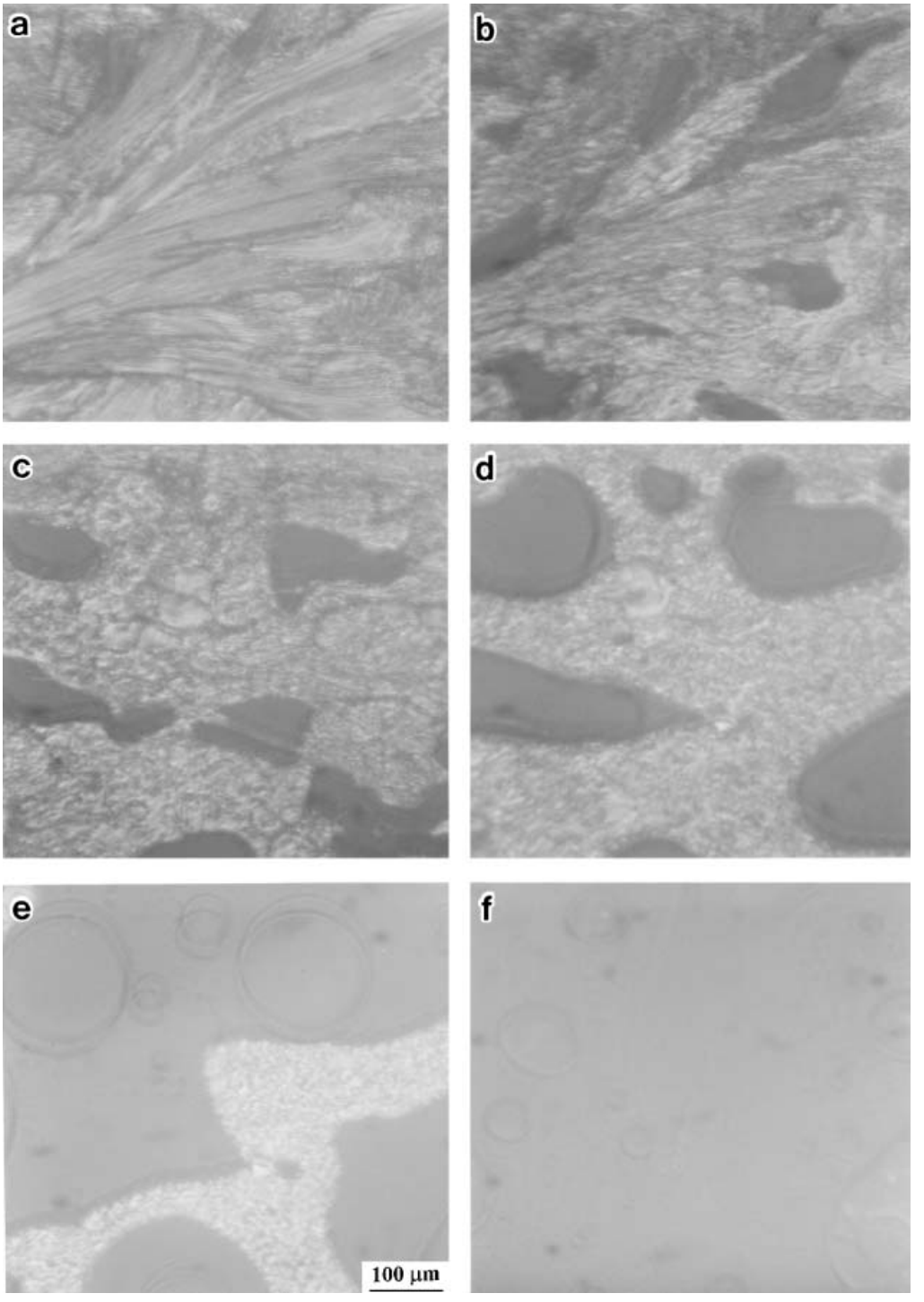

Figure 6. POM photographs of BABH(12) on heating at 30 MPa: (*a*) Cr_3 at 30°C; (*b*) Cr_1 at 141°C; (*c*,*d*) sea–island texture of the bright sea (SmC phase) and dark islands (cubic phase) at 157 and 164°C; (*e*) SmC phase and isotropic liquid at 166°C; (*f*) isotropic liquid at 167°C.

~10 microns, respectively. When the pressure is raised to 12 MPa, several dark regions are formed, figure 8 (*c*), and these grow gradually with time, indicating the completion of the sand-like texture of the pressure-induced SmC phase after 5 min, figure 8 (*d*). The morphological change seen for

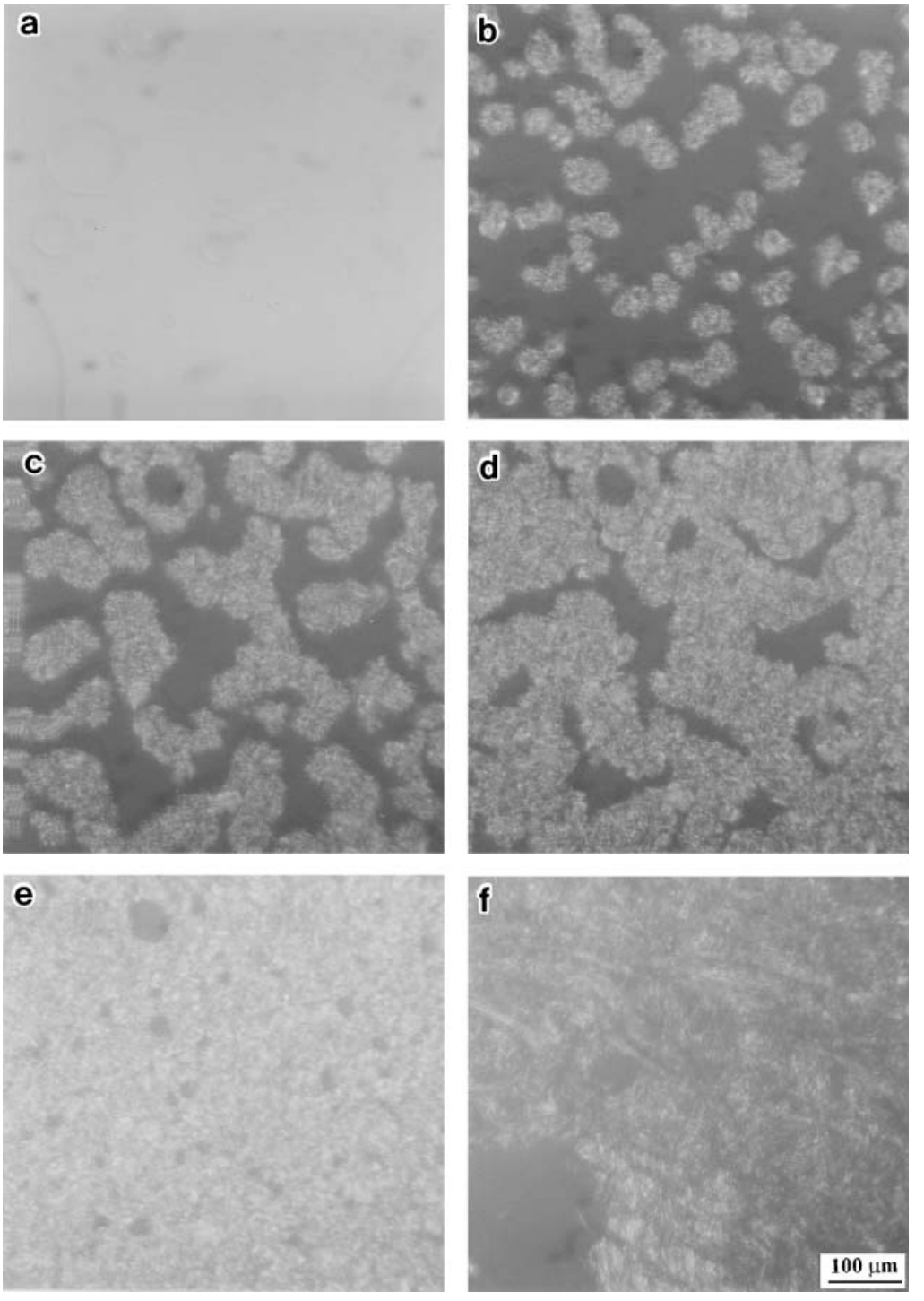

Figure 7. POM photographs of BABH(12) on the subsequent cooling at 30 MPa: (*a*) isotropic liquid at 168°C; (*b*) pressure-induced formation of the SmC phase at 166°C; (*c*,*d*) growth of the island texture (SmC phase) at 164 and 163°C; (*e*) SmC phase at 157°C; (*f*) Cr_1 phase at 34°C.

BABH(11) at 145 and 150°C also occurs at about 12 MPa, indicating that the transition between the cubic and SmC phases is largely independent of temperature. The change in texture is reversible on an isothermal path: figures 8 (*e*) and 8 (*f*) clearly show the change from sand- to the mesh-like textures on depressurizing at 140°C. The same morphological phenomenon is seen for BABH(12). In BABH(12) the morphological

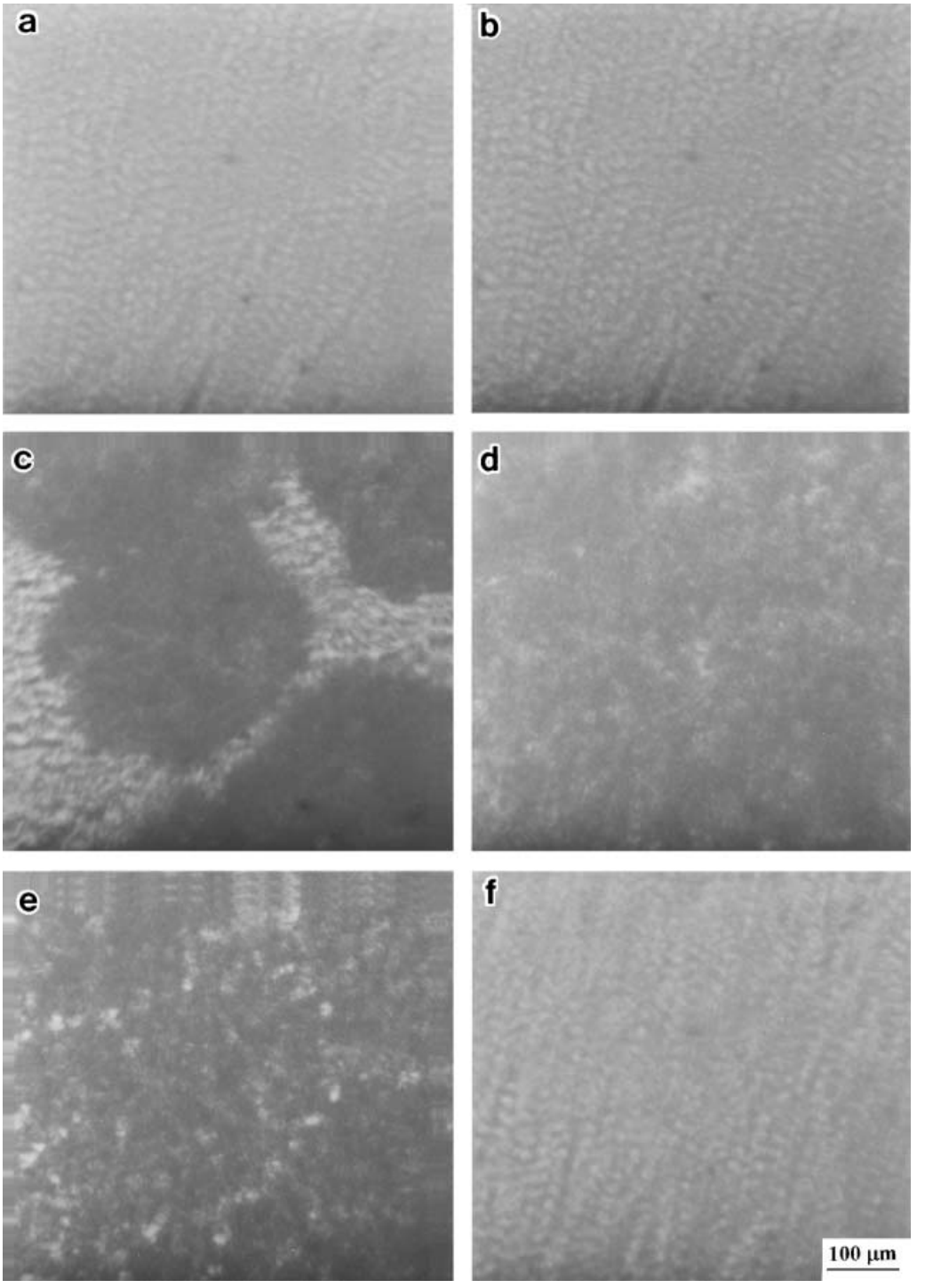

Figure 8. POM photographs of BABH(11) in an isothermal path at 140°C: (*a*,*b*) mesh-like texture of the cubic phase at 3 and 10 MPa; (*c*) Cub–SmC transition at 12 MPa; (*d*) sand-like texture of the SmC phase at 140°C after 5 min; (*e*) SmC–Cub transition at 10 MPa with decreasing pressure; (*f*) mesh-like texture of the cubic phase at 4 MPa.

transition between mesh- and sand-like textures occurs at about 16–17 MPa. It is clear from the series of *in situ* morphological observations that the SmC phase is induced between the isotropic liquid and the cubic phase under pressures of about 10–12 and 16–17 MPa in BABH(11) and BABH(12), respectively, while the SmC phase does not appear at lower pressures including atmospheric pressure. The SmC phase exists

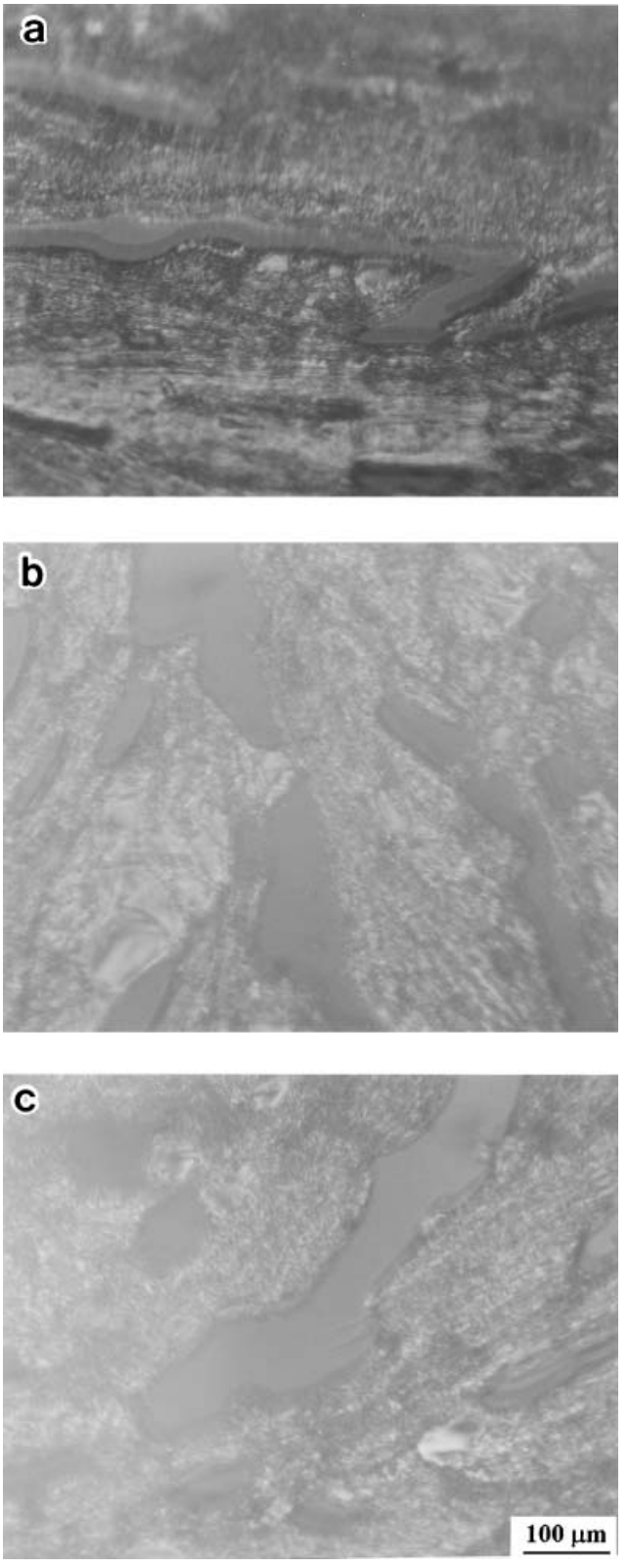

Figure 9. POM photographs of the sea–island textures at high pressures: (*a*) BABH(11) at 153°C, 50 MPa; (*b*) BABH(12) at 150°C, 50 MPa; (*c*) BABH(12) at 195°C, 140 MPa.

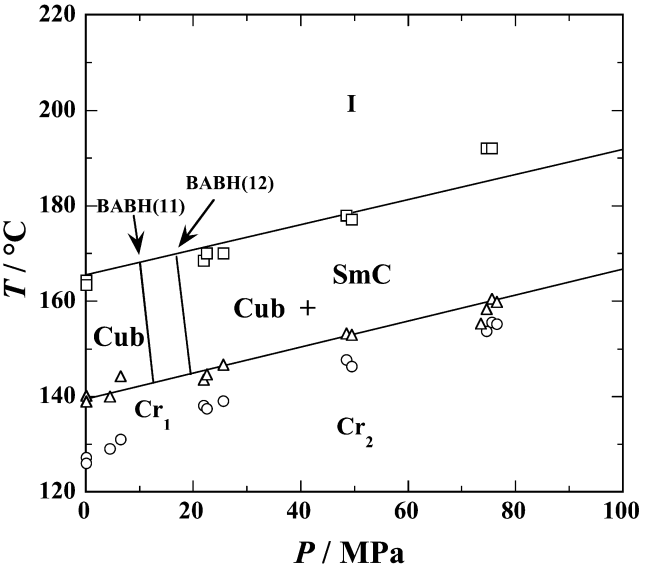

Figure 10. Schematic *T*–*P* phase diagram of BABH(11) and BABH(12) showing the boundary pressures and also the region of the co-existent sea (SmC)–island (Cub) texture. The lower limits of pressure for the formation of the pressure-induced SmC phase are determined using *in situ* POM observations under hydrostatic pressure.

preferably at high pressures above the boundary pressures, but at the same time co-exists with the minor component of the cubic phase on heating over a wide pressure range.

The sea–island textures of BABH(11) and BABH(12) are observed under elevated pressures up to 140 MPa, see figure 9. In consequence, the triple points, such as those found in BABH(8) and BABH(10), indicating the upper limit of pressure for observation of the cubic phase, have not yet been determined for BABH(11) and BABH(12). Figure 10 is schematic phase diagram showing the boundary pressures and the co-existence region of the cubic and SmC phases. The boundaries between the pure cubic phase and the coexistent Cub and SmC phases in the high pressure region are shown as almost vertical lines for BABH(11) and BABH(12), indicating the lower limits of pressure for the formation of the SmC phase as a high pressure phase.

The X-ray patterns of BABH(11) and BABH(12) observed under pressures correspond well to the *in situ* POM morphological observations. Figure 11 shows the effect of pressure on the X-ray diffraction pattern and the texture of the cubic phase of BABH(12) at 150°C. The spot-like pattern (*a*) and mesh-like texture (*d*) of the cubic phase at 10 MPa change reversibly to the continuous Debye–Sherrer pattern (*c*) at 30 MPa and (*f*) sand-like texture at 17 MPa for the SmC phase, via an intermediate stage (*b*) of the diffraction spots overlapped with the continuous reflection and (*e*) an

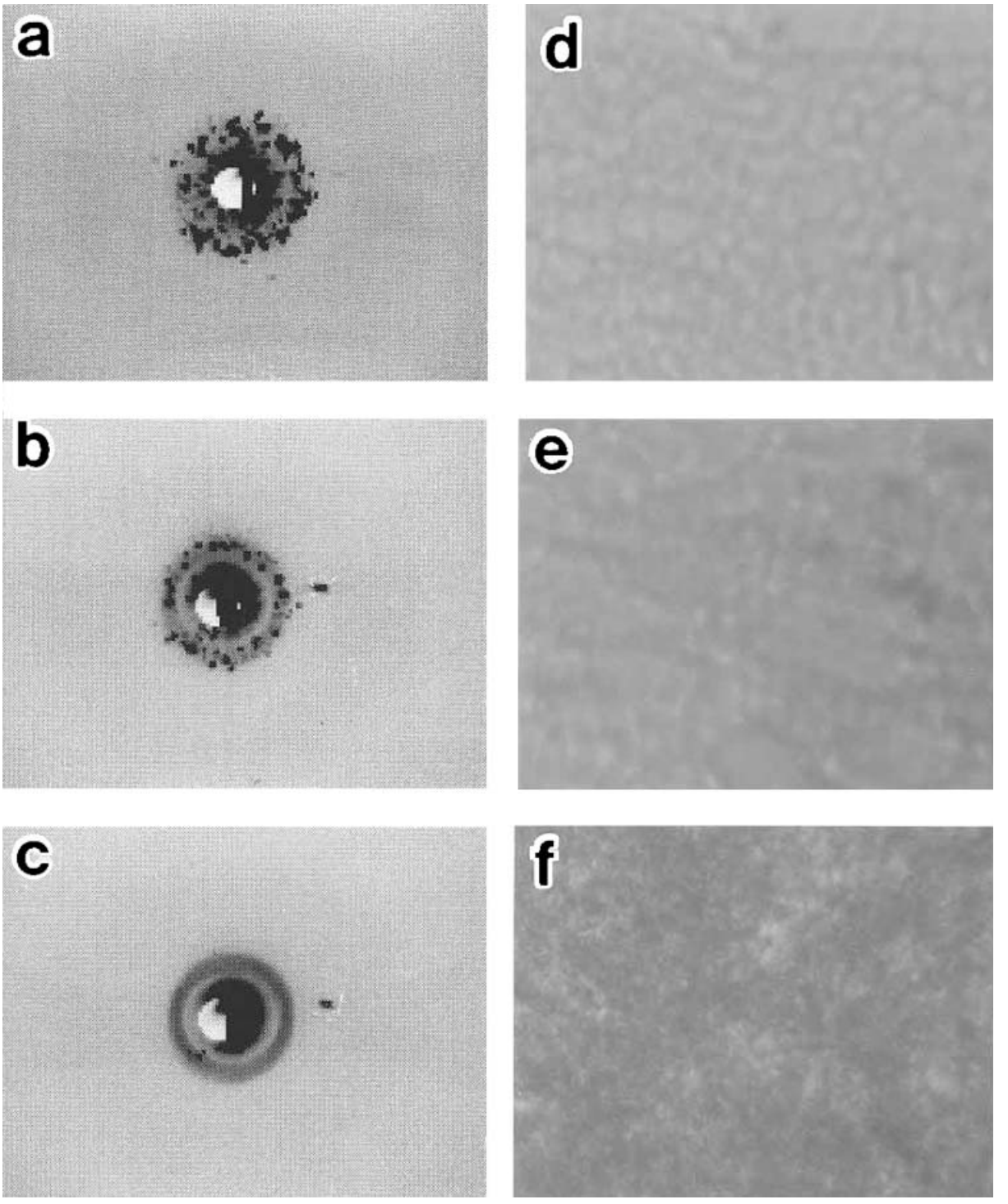

Figure 11. Pressure dependence of the X-ray diffraction patterns of BABH(12) at 150°C. The spot-like diffraction patterns of (*a*) the cubic phase at 10 MPa change reversibly to (*c*) the Debye–Sherrer pattern of the (0 0 1) reflection of the SmC phase at 30 MPa. (*d*) Mesh-like texture of the cubic phase and (*f*) sand-like texture of the smectic C phase, (*b*) and (*e*) are the X-ray patterns and optical texture for a biphasic region at 15 MPa.

ambiguous texture at 15 MPa. The structural change between the cubic phase and the lamellar structure (SmC) at 150°C occurs mainly at pressures between 15 and 20 MPa, corresponding to the morphological changes between the mesh- and the sand-like textures. Several low angle reflections for the cubic phase are observed at $2\theta = 2.98°$ ($d = 2.96$ nm) and $2\theta = 3.40°$ ($d = 2.59$ nm), while the (0 0 1) reflection of the SmC phase at 150°C is observed at $2\theta \cong 3.04°$ ($d = 2.90$ nm).

The predominance of the SmC phase over the cubic phase for BABH(8) and BABH(10) under pressure is explained thermodynamically using the criteria of the Gibbs energy–T relation shown schematically in figure 12. The Gibbs energy of the cubic phase shifts to higher values with increasing pressure, which means the destabilization of the cubic phase with increasing pressure. As a result the SmC phase becomes stable between the crystal and the isotropic liquid under pressure. The same situation may also pertain for BABH(11) and BABH(12), as shown in figure 12. In other words, the Cub–SmC transition in BABH(8) and BABH(10) may be explained using the Clausius–Clapeyron equation. The molar volume is estimated to decrease at the Cub→SmC transition [25, 26]: the molar volume of the high temperature SmC phase will be smaller than that of the low temperature cubic phase, i.e. $V_{SmC} < V_{Cub}$. The molecular aggregation under pressure is better for the densely packed SmC phase than for the cubic phase because the relationship $\Delta V < 0$ for the Cub–SmC transition under pressure is implied.

For BABH(11) and BABH(12) the plausibility of this explanation is less certain because the Clausius–Clapeyron equation is not applicable due to the absence of the Cub–SmC transition line at atmospheric pressure and a true Cub–SmC transition has not yet been determined. However the same situation would be expected in BABH(11) and BABH(12). The Cub–SmC transition induced by applying pressure is schematically illustrated in figure 13. The cubic phase is constructed using either the jointed-rod models [3–7] or the densely packed and three-dimensionally connected IPMS structure [8–13]. It is suggested that the net volume of the cubic phase is primarily determined not by the highly disordered alkyl chains but by the densely packed and three-dimensionally connected IPMS structure [17, 18].

4. Conclusion

The phase transition behaviours of BABH(11) and BABH(12) were investigated under hydrostatic pressures up to 300 MPa using a high pressure DTA, a polarizing optical microscope equipped with a high pressure optical cell, and the WAXD apparatus equipped with a high pressure vessel. The temperature versus pressure phase diagrams of BABH(11) and BABH(12) were constructed. The phase sequence for BABH(11) and BABH(12) may be summarized thus: the SmC phase is induced preferably as a high pressure phase and exists concurrently with a minor component of the cubic phase under pressure. The dark brown field of view for the optically isotropic cubic phase changes reversibly to the sand-like texture of the SmC phase under both isobaric and isothermal conditions. The spot-like X-ray pattern of the cubic phase at atmospheric and low pressures changes reversibly to the Debye–Sherrer pattern of the SmC phase at high pressures. The phase transition occurs reversibly via the sequence Cr_3–Cr_2–Cr_1–Cub–I under low pressures

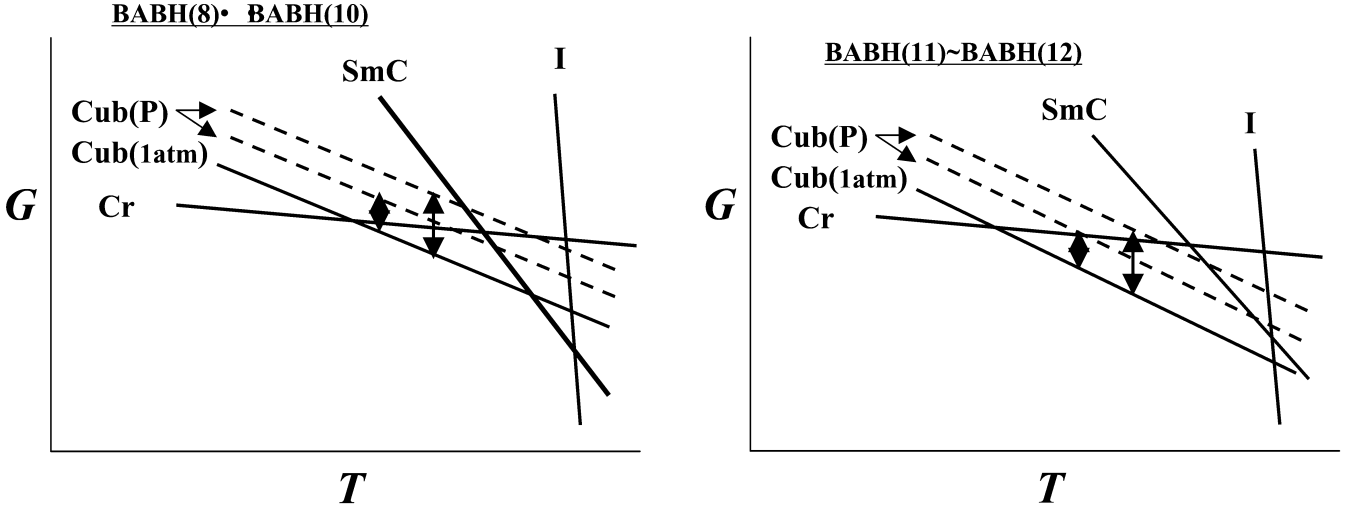

Figure 12. Schematic diagram of the Gibbs energy–T curve. The energy line for the cubic phase shifts to higher levels with increasing pressure. The cubic phase is destabilized under pressure, while the SmC phase becomes comparatively stable under pressure.

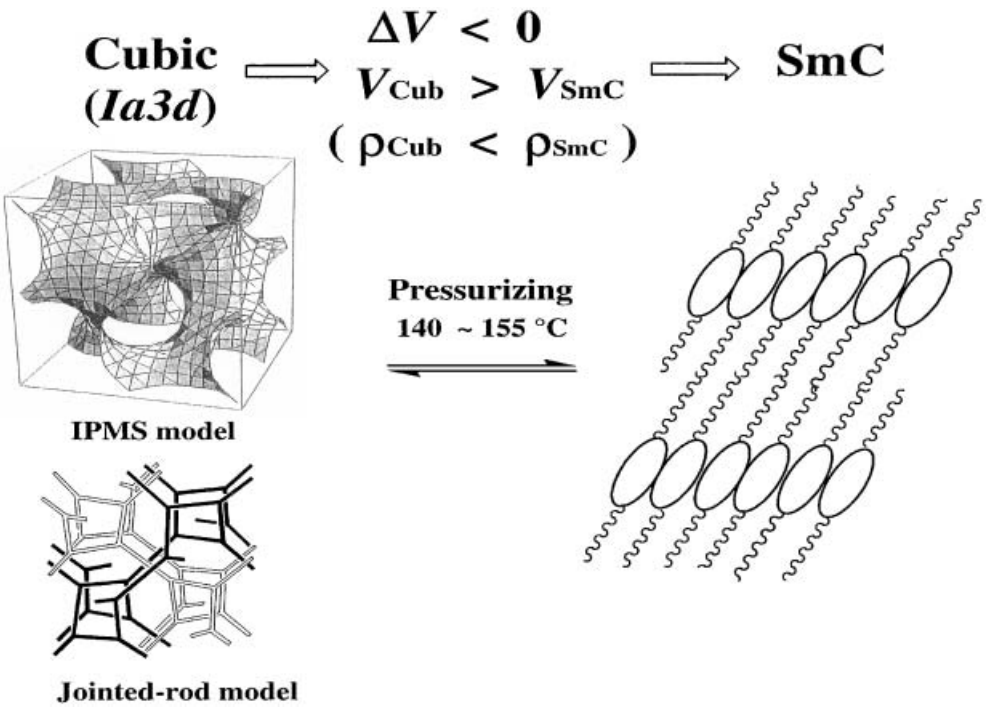

Figure 13. Schematic drawing of the Cub–SmC transition induced by applying pressure for BABH(n, n=8–12).

below 10–12 and 16–17 MPa for BABH(11) and BABH(12), respectively. The transition occurs via the sequence Cr_2–Cr_1–SmC(coexistent with Cub)–I in the intermediate pressure region between 10–20 and 150 MPa; the transition sequence of Cr_2–SmC–I then appears in the high pressure region.

K.S. is grateful for financial support from the Ministry of Education, Culture, Sports, Science and Technology, Japan (Grant-in-Aid for Scientific Research No. 413/13031037 and 14045232, and (C) 14550846).

References

[1] Schubert, H., Hauschild, J., Demus, D., and Hoffmann, S., 1978, *Z. Chem.*, **18,** 256.
[2] Demus, D., Gloza, A., Hartung, H., Hauser, A., Rapthel, I., and Wiegeleben, A., 1981, *Cryst. Res. Technol.*, **16,** 1445.
[3] Luzzati, V., and Spegt, A., 1967, *Nature*, **215,** 701.
[4] Luzzati, V., Tardieu, A., Gulik-Krzywicki, T., Rivas, E., and Rerss-Hussom, F., 1968, *Nature*, **220,** 485.
[5] Spegt, P. A., and Skoulios, A. E., 1966, *Acta Cryst.*, **21,** 892.
[6] Tardieu, A., and Billard, J., 1976, *J. Phys. (Paris) Colloq.*, **37,** C3–79.
[7] Levelut, A.-M., and Clerc, M., 1998, *Liq. Cryst.*, **24,** 105.
[8] Charvolin, J., and Sadoc, J. F., 1990, *Colloid polym. Sci.*, **268,** 190.
[9] Seddon, J. M., Hogan, J. L., Warrender, N. A., and Pebay-peyroula, E., 1990, *Progr. colloid polym. Sci.*, **81,** 189.
[10] Seddon, J. M., and Templer, R. H., 1993, *Phil. Trans. r. Soc. London*, **344,** 377.
[11] Schön, A. H., 1969, *Not. Am. math. Soc.*, **16,** 519.
[12] Hyde, S. T., Anderson, S., Ericsson, B., and Larson, K., 1984, *Z. Kristallogr.*, **168,** 213.
[13] Schwarz, H. A., *Gesammelte Math. Abhandlungen*, Bd. I. (Berlin: Springer), p. 1890.
[14] Diele, S., and Göring, P., 1998, in *Handbook of Liquid Crystals*, Vol. 2B, edited by D. Demus, J. Goodby, G. W. Gray, H.-W. Spiess and V. Vill (Weinheim: Wiley-VCH), p. 887.
[15] Clerc, M., and Dubois-violette, E., 1994, *J. Phys. II Fr.*, **4,** 275.
[16] Göring, P., Diele, S., Fischer, S., Wiegeleben, A., Pelzl, G., Stegemeyer, H., and Thyen, W., 1998, *Liq. Cryst.*, **25,** 467.
[17] Saito, K., and Sorai, M., 2002, *Chem. Phys. Lett.*, **366,** 56.
[18] Sorai, M., and Saito, K., 2003, *Chem. Rec.*, **3,** 29.
[19] Sato, A., Yamamura, Y., Saito, K., and Sorai, M., 1999, *Liq. Cryst.*, **26,** 1185.
[20] Saito, K., Shinhara, T., Nakamoto, T., Kutsumizu, S., Yano, S., and Sorai, M., 2002, *Phys. Rev. E*, **65,** 031 719.
[21] Saito, K., Sato, A., and Sorai, M., 1999, *Liq. Cryst.*, **25,** 525.
[22] Morimoto, N., Saito, K., Morita, Y., Nakasuji, K., and Sorai, M., 1999, *Liq. Cryst.*, **26,** 219.
[23] Saito, K., Sato, A., Morimoto, N., Yamamura, Y., and Sorai, M., 2000, *Mol. Cryst. liq. Cryst.*, **347,** 249.
[24] Saito, K., Shinhara, T., and Sorai, M., 2000, *Liq. Cryst.*, **27,** 1555.

[25] MAEDA, Y., SAITO, K., and SORAI, M., 2003, *Liq. Cryst.*, **30,** 1139.
[26] MAEDA, Y., ITO, T., and KUTSUMIZU, S., 2004, *Liquid Crystals*, **31,** 623.
[27] ITO, T., and KUTSUMIZU, S., 2003, Bachelor thesis, Faculty of Engineering, Gifu University, Japan.
[28] MAEDA, Y., and KANETSUNA, H., 1985, *Bull. Res. Inst. Polym. Tex.* **149**, 119; MAEDA, Y., 1990, *Thermochim. Acta*., **163**, 211.
[29] MAEDA, Y., and KOIZUMI, M., 1996, *Rev. sci. Instrum.* **67**, 2030; MAEDA, Y., and KOIZUMI, M., 1998, *Rev. high pressure Sci. Technol*., **7**, 1532.